

# AguaClara Cornell Floc Modeling

## Spring 2025: Final Report

Anjali Asthagiri (aa2549), Isabel Crovella (isc25), Alex Gardocki (rag325), Lauren Hsu (lkh58),

Max Zheng (hz687)

May 2, 2025

## Abstract

Most surface water treatment plants, including AguaClara technology, rely on flocculation and clarification processes for particle aggregation and removal. This research project aims to develop a mathematical model of these processes that can be applied to optimize the design of treatment plants and reduce operating costs. There are two main focus areas for this project: investigating and predicting (I) floc filter dynamics during clarification and (II) particle collisions during flocculation. Specifically, the Spring 2025 Floc Modeling team aims to develop an understanding of the spatial distribution of floc saturation in the floc filter. The team is designing and conducting experiments with a miniature clarifier to visualize gradients in floc saturation within the floc filter, correlate floc filter saturation state with primary particle removal performance, and analyze how influent turbidity and coagulant dose conditions affect floc saturation. To further develop the flocculation model, the team is introducing new mechanisms to the model, including coagulant attachment to the flocculator walls and coagulant attachment to other coagulant nanoparticles. The improved flocculation and clarification models will be applied to automate coagulant dosing in collaboration with the Automated Coagulant Dosing Controller (ACDC) subteam.

## Introduction

Effective water treatment is essential for public health and the welfare of communities. Untreated water typically contains small primary particles made of silt, clay, and sand ( $<1\text{ }\mu\text{m}$  diameter) and dissolved organic matter (DOM) such as plant and animal material, algae, and bacteria. In the AguaClara treatment process, flocculation and clarification processes are critical, as they remove most of these particles before filtration and chlorination. While these processes are widely used throughout the water treatment industry, gaps remain in our understanding of their underlying physical mechanisms. This lack of understanding has made it challenging to optimize the design of treatment plants and develop automated systems that can successfully respond to fluctuating conditions. As a result, water treatment facilities may experience inefficiencies that not only reduce performance, but also result in high operational costs.

The framework of AguaClara's current understanding of flocculation and clarification is as follows. Flocculation combines primary particles into larger aggregates called flocs (10-500  $\mu\text{m}$  diameter), which can more easily be removed through gravity-driven sedimentation. For flocs to form successfully, a coagulant particle must be present at the point of contact since it

enables covalent bonding between clay particles and is therefore necessary for successful clay-clay attachment. Hence, a sufficient amount of coagulant must be added prior to flocculation for this process to be effective. However, adding too much coagulant is wasteful and overdosing failures have been observed.

Clarification follows flocculation. It is a process that allows the newly formed flocs to settle and separate from the treated water. During conventional clarification, flocs settle and are wasted. In order to increase the efficiency of clarification, AguaClara plants utilize a process called floc sweeping, where previously formed flocs capture additional primary particles in a suspension called a floc filter. Water jets maintain the water flow in the floc filter and guide smaller flocs through the floc filter and towards the plate settlers. These angled plates help smaller flocs aggregate further and eventually settle back into the floc filter.

Floc sweeping efficiency depends on coagulant dose, floc filter concentration, and floc saturation. As a floc captures primary particles, its pores fill. Once the floc is fully saturated, it cannot capture additional particles. Spatial variations in floc saturation within the clarifier can affect particle removal efficiency in the clarifier.

While the processes of flocculation and clarification are fundamental to water treatment, they are also complex, with many underlying mechanisms still not fully understood. The interactions between coagulant dose, floc formation, and particle capture involve a range of physical and chemical variables that make it difficult to predict and optimize performance. A mathematical model is essential for addressing these uncertainties, particularly in three key areas: (1) automating coagulant dosing, (2) optimizing clarifier design by managing floc saturation, and (3) improving flocculator design to enhance particle aggregation. An effective model must be both accurate and simple as it ensures that the model can be applied in real-world settings to inform design decisions and automate treatment processes. Current models, however, require further refinement to achieve this goal, as will be discussed in the Literature Review section below.

## Literature Review & Previous Work

### Flocculation Modeling with Charge Neutralization Theory

The successes and failures of past flocculation models must be considered in order to investigate the mechanisms of flocculation. To understand how to model flocculation, the first mechanism to consider is coagulant function. The coagulant used for experimentation, Poly-Aluminum Chloride (PACl), forms sticky hydroxide nanoparticles in the solid phase when diluted with water as seen in Equation 1.



Previous flocculation models are based on Charge Neutralization Theory (CNT) or DLVO Theory, which explain why there is an optimal coagulant dosage for a certain amount of charged particles present in untreated water (Runkana 2004). The theory explains that the

amount of charge contributed by the positive metal cation  $\text{Al}^{3+}$  effectively neutralizes the negative charges of the clay primary particles, allowing them to join together and eventually form flocs under appropriate collision conditions.

Figure 1a demonstrates the electrical double layer (EDL), measured by the Nernst potential. Constituted by the Stern potential and the zeta potential, the Nernst potential is a measure of the total electrical potential at the surface of a particle. Due to charged particles wanting to achieve electrical neutrality, positive ions from the solution group around the negatively-charged primary particle to form the Stern layer. The Stern layer directly contributes to the Stern Potential, which is the decrease in the electric potential of the primary particle due to the gathering of positive charges in the Stern layer.

As more coagulant is added, the Stern layer increases in charge, decreasing the Zeta potential and compressing the EDL by making the initial electrostatic potential gradient much steeper. The Zeta potential represents the repulsive force from the primary particle, and so as it decreases, the probability of collision between two primary particles with low Zeta potentials increases. This idea is demonstrated by the unstable system seen in Figure 1b, which is preferable for flocculation compared to the stable system. The unstable system has a lower resultant force as a function of the distance between two primary particles, and so they are more likely to collide and aggregate.

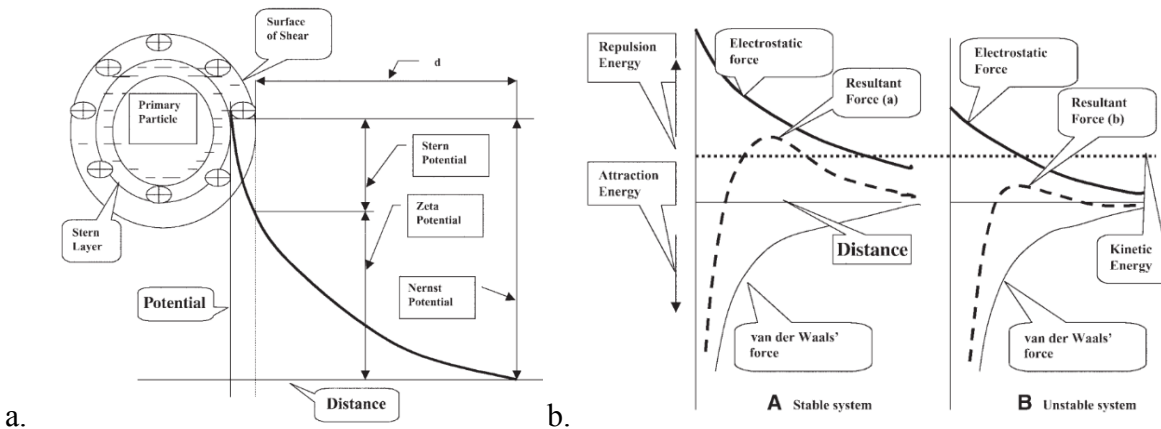


Figure 1. From Shammas, Nazih K. demonstrating (a) the electrical potential of a negatively charged colloidal particle, and (b) the effect of interparticle forces on the stability of a colloidal system. (2005)

While CNT is correct in its beliefs that the addition of coagulant helps to compress the EDL and lower the zeta potential, it fails to fully meet a few observed flocculation tendencies. For example, at high turbidities, lower dosages of coagulants relative to turbidity work just as effectively compared to low turbidities despite a measure of the zeta potential not indicating full neutralization of charges or a stoichiometric relationship. Instead, Chen et al. (2006) demonstrated that when dosed linearly with turbidity, observations such as the formation of smaller flocs indicate an overdosing failure, resulting in a destabilization of the floc filter.

Another oversight of the CNT stems from its assumptions about coagulant functionality. Since the CNT believes coagulant only contributes charge neutralization, it leads to the conclusion that once two primary particles overcome their EDLs, the bonds holding together particles are simply intermolecular van der Waals forces. However, this cannot be true as throughout the flocculation process, aggregations of particles experience forces much higher than van der Waals forces. According to Swetland et al., this means flocculation would cause particles to separate after aggregation under CNT, despite flocculation being the primary reason for particle aggregation (2014). Another shortcoming of CNT is its lack of consideration for the rapid mixing process, which plays a crucial role in determining flocculation success. As shown by Swetland et al. (2013), delayed or insufficient mixing after coagulant dosing allows polymeric aluminum oxyhydroxide precipitates to self-aggregate before interacting with colloidal particles. This aggregation reduces surface coverage on clay particles, decreases attachment efficiency, and leads to poor turbidity removal. Therefore, effective flocculation requires vigorous and immediate mixing of coagulant into the raw water to minimize coagulant-coagulant aggregation and ensure optimal interaction with colloids. The last observation CNT fails to explain is the formation of coagulant flocs in deionized water. Without any clay or other floc-forming particles present, the injection of pure coagulant still leads to the observed formation of flocs which are theorized to be comprised of coagulant-coagulant bonds by Swetland et al. (2013).

These shortcomings of the CNT lead to the hypothesis that Charge Neutralization Theory is not capable of fully explaining the formation of flocs due to coagulant. This shifted the focus of flocculation modeling towards collision-based models, where flocculation is driven by the frequency and attachment efficiency of particle collisions rather than the charge of the particles.

## Flocculation Modeling with a Collision-Based Approach

The flocculation model developed by Argaman and Kaufman (1970) offers a conceptual basis for describing the competition between particle aggregation and floc breakage. However, the model is constrained by several assumptions that limit its accuracy and applicability. The model tracked the concentration of primary particles, which cannot be directly measured, and assumed that particle movement is governed by large-scale eddies and that small particles collide with larger aggregates. These assumptions were later refuted by Casson and Lawler (1990), who showed that collisions are primarily driven by small-scale eddies and typically occur between particles of similar sizes. Additionally, Argaman and Kaufman (1970) and Liu et al. (2004) demonstrated that floc breakup has a negligible role compared to aggregation, further undermining the model's premise. The practical application of the model is also limited by its reliance on empirical constants, which are influenced by influent turbidity and coagulant dosage (Haarhoff & Joubert, 1997).

Lee et al. (2000) and Casson and Lawler (1990) applied the Smoluchowski (1917) model to describe particle distribution during flocculation, relying on parameters for collision frequency and efficiency. Although this approach introduced a more granular perspective on particle interactions, it required simplifying assumptions to render the equations usable. The parameters

are highly system-specific and do not account for critical physical and mechanistic factors, reducing the adaptability of the model to varying conditions.

More recently, computational fluid dynamics (CFD)-based approaches have modeled spatial velocity gradients. Studies have shown that extreme gradients, rather than average values, dominate floc breakage, making spatially-resolved CFD models particularly valuable (Bridgeman et al., 2009). Nevertheless, CFD models are computationally intensive and often impractical for exploring a wide range of design conditions.

The mechanistic model introduced by Pennock et al. (2018) and Du et al. (2019) presents a promising advancement. This model describes the transformation of non-settleable particles into settleable flocs—a measurable quantity—and depends primarily on physical rather than empirical constants, making it more adaptable. Du et al. (2019) expanded the model to consider the influence of dissolved organic matter on collision efficiency. While the model has demonstrated practical value, particularly for informing flocculator design and predicting settled turbidity, discrepancies with experimental findings have been observed (Tse et al., 2011). The model may be limited by not accounting for coagulant-coagulant and coagulant-wall collisions, the relative strengths of coagulant-coagulant and coagulant-clay bond strengths, and the finite strength of particle bonds at the time of collision. Therefore this study will focus on expanding the model to include these mechanisms in order to enhance the predictive accuracy of the model.

## Clarification Modeling

Vitasovic (1986) and Takacs et al. (1991) developed a 1D model of clarification based on solids flux theory to predict the sludge blanket settling velocity. The Takacs model unified the description of both discrete and hindered settling into a single equation. However, Gernaey et al. (2001) highlighted the difficulty of fitting this model, limiting its utility in practical applications. Head et al. (1997) modeled floc blanket clarification by examining how influent concentration and floc wastage flow rate influence the height and concentration of the floc blanket. However, the model is limited in its ability to describe how particle size distribution post-flocculation and coagulant dosage impact clarification performance.

Sarmiento (2021) addressed this gap by applying the Pennock et al. (2018) flocculation model which accounts for coagulant dosage and distinguishes between the settleable and non-settleable particles formed during flocculation. Sarmiento (2021) assumes that all settleable particles generated during flocculation are removed during clarification. In contrast to model predictions, experimental results indicate that clarification performance decreases over time, possibly due to effects of floc saturation. Pennock et al. (2024) modified the Pennock et al. (2018) flocculation model to describe how the conversion from non-settleable to settleable particles depends on clarifier design. Nonetheless, their work did not incorporate floc sweeping and floc saturation, which are of significance in floc filter-based clarifiers. In the summer of 2024, our team built on these models to account for floc sweeping and floc saturation. Despite these enhancements, discrepancies between experimental and theoretical parameter values exist, indicating the need to reevaluate the assumptions of the model (Appendix Section I). The major

assumptions are that flocs in the floc filter are at their steady-state saturation level and the floc filter is well-mixed. Therefore experimentation is needed to investigate the spatial and temporal dynamics of the floc filter. This semester, the subteam is specifically focused on understanding the dynamics of floc saturation within the clarifier.

## Part I: Experimentation

### Methods

#### Experimental Setup

In order to experimentally guide our development of models for flocculation and clarification, and specifically to investigate floc saturation within the floc filter, we designed a small-scale, low-hydraulic residence time clarifier to allow for a novel approach to visualizing floc saturation. In the experimental setup, a white clay stock solution and coagulant first flows through a tube flocculator. After exiting the flocculator, a red kaolin clay stock solution is added to the stream and pumped into the clarifier. This serves to add colored primary particles to the clarifier influent. Within the clarifier, the flocs formed from the white clay and coagulant settle to form a floc filter that captures the red clay primary particles through floc sweeping. Excess flocs overflow into the floc hopper to be drained. A set of plate settlers provides additional surface area to aggregate small flocs and reintroduce them to the floc filter. Effluent exits above the plate settlers.

In this setup, the coloration of the floc filter may provide insights into the spatial distribution of floc saturation. Capturing additional primary particles increases the saturation of a floc, so flocs which have captured more of the red clay primary particles will be more saturated. Hence, a region having a stronger coloration relative to the rest of the floc filter may indicate that the flocs in that region are more highly saturated.

When designing our miniature clarifier, we attempted to capture the characteristics of a full size AguaClara plant while allowing for modifications to test different conditions. For example, the diffuser inlet uses a threaded adapter which screws into the clarifier. Since this inlet adapter is resin-printed, new adapters with different sizes and diffuser shapes can be printed easily, giving us control over influent velocity and the initial velocity gradient in the clarifier. The current diffuser inlet widens outward so that the influent velocity is consistent between cross-sections parallel to the viewing plane. To prevent interference with the floc filter, rather than being directed downward toward the jet reverser, the jet enters from the side and is redirected 90° by the jet reverser, which is shaped as a quarter circle. The angle of the diffuser is 50°, consistent with AguaClara plants (Weber-Shirk, n.d.). The height of the floc filter is 134 mm.

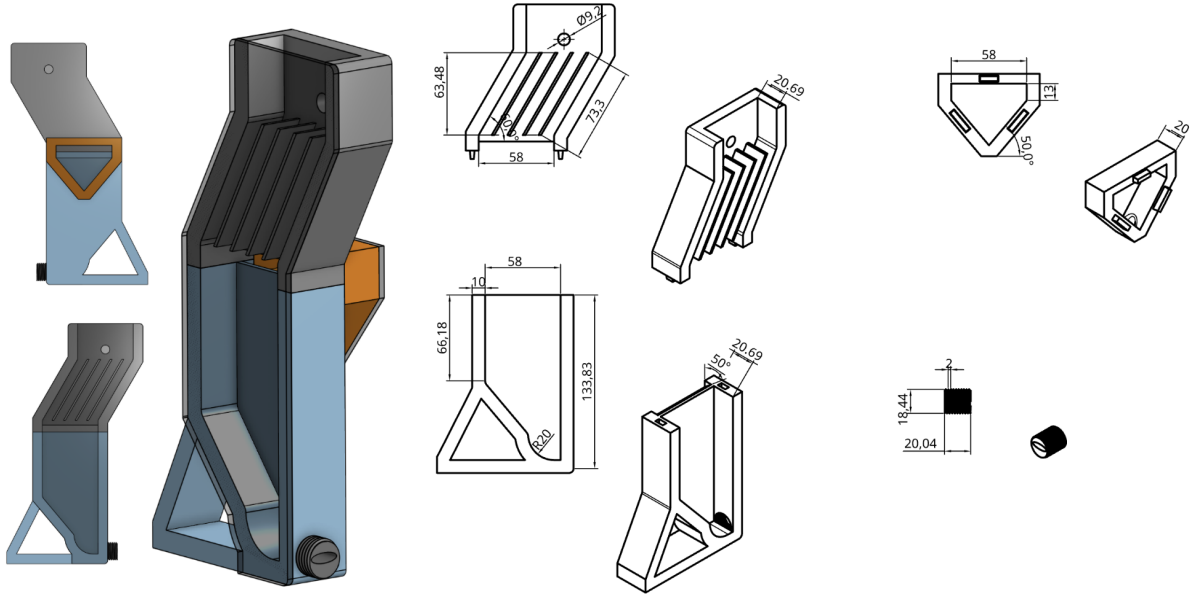


Figure 2. Clarifier schematic. Dimensions are in millimeters.

For the upflow velocity, 1 mm/s was chosen based on the specifications for AguacLara plants (Weber-Shirk, n.d.). Given the targeted flow rate of 1.2 mL/s based on the Dissolved Organic Matter (DOM) subteam's prior work with the tube flocculator, the cross-sectional area of the clarifier was designed to be 1200 mm<sup>2</sup>. An initial influent velocity of 21 mm/s through the diffuser was chosen in order to have sufficient speed to keep the floc filter suspended. To achieve this, a cross sectional area of 57.55 mm<sup>2</sup> was chosen for the diffuser inlet.

For the plate settlers, a spacing of 1 cm between plates was chosen to avoid floc rollup. Using the equation found in the AguacLara textbook (Weber-Shirk, n.d.), we calculated the necessary plate settler length to be 14.667 cm to ensure the AguacLara standard capture velocity of 0.12 mm/s. However, due to limitations in print size, we chose to reduce the length to 7.33 cm, resulting in a capture velocity of 0.73 mm/s. A plate width of 2.0 mm was chosen to balance the integrity of the print with having the thinnest plates possible to reduce the increase in upflow velocity through the plate settlers. The plates were placed at a 60° angle based on AguacLara clarifier specifications (Weber-Shirk, n.d.). The area above the plate settlers was left open to the air to prevent air bubbles from being trapped in a closed system.

Lastly, we added a floc weir connected to a floc hopper in order to remove excess flocs from the floc filter. We utilized the same clear acrylic on the hopper as the front of the clarifier in order to visualize when the floc hopper must be emptied. Pumps are used to remove waste from the floc hopper and effluent from the top of the clarifier.

## Experimental Design

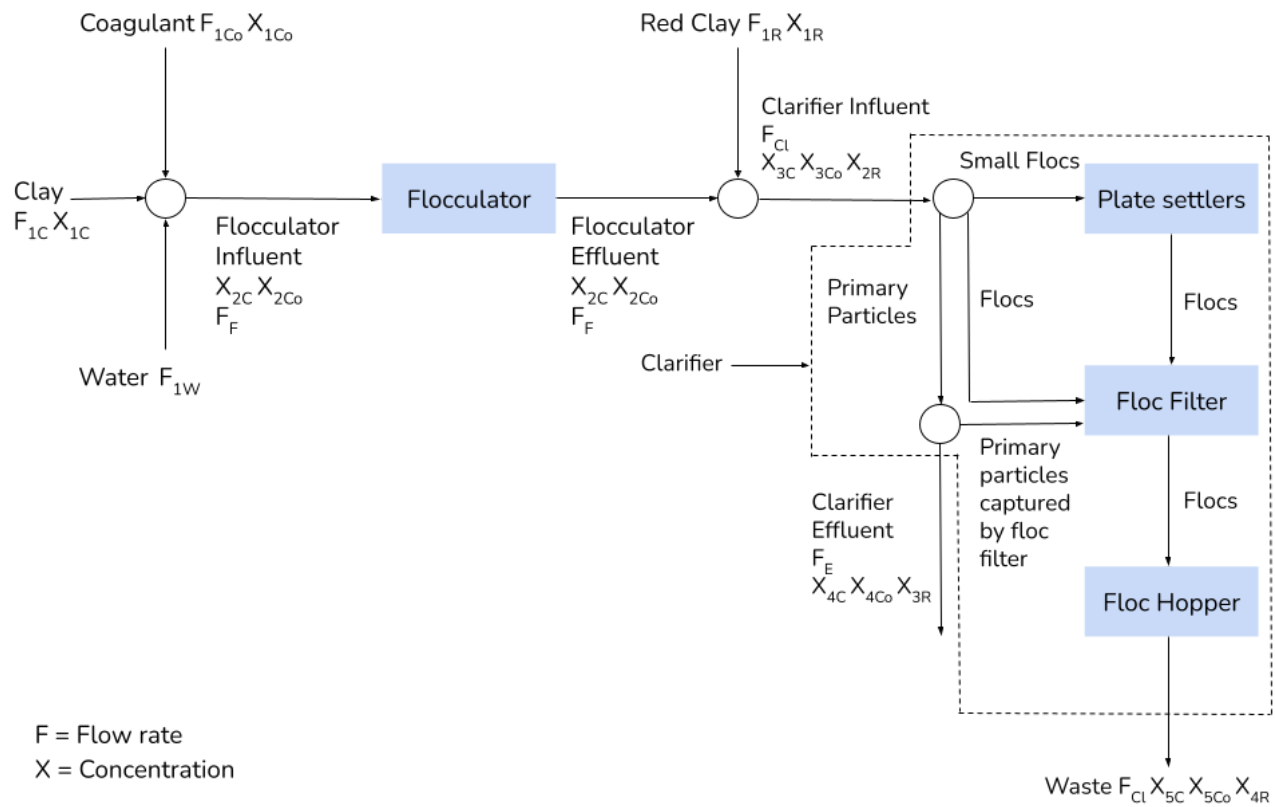


Figure 3. Process flow diagram illustrating movement of clay, coagulant, and red clay through the experimental setup.



Figure 4. Picture of experimental setup in lab. The clarifier is seen mounted on the bottom left.

A mass balance calculator was created to determine flow rates and pump speeds in the experimental setup shown in Figure 3. The mass balance calculator takes inputs for stock concentrations and clarifier influent concentrations of coagulant, clay, and red clay and the flow rate of the waste pump. Flow rates are calculated using the total clarifier influent flow rate (1.2 mL/s), stock concentration, and target clarifier influent concentration. Pump speeds are then determined using the flow rates and volume per revolution for each pump. See Appendix II for mass balance calculations.

For all experiments, the floc filter will be grown rapidly in the clarifier with a higher influent turbidity and coagulant dosage, before transitioning to standard influent and coagulant conditions and adding red clay. The expected time to grow a floc filter is 29.33 minutes, which was calculated using Equation 2.

$$Floc\ filter\ growth\ time = \frac{A_{Clarifier\ cross-sectional\ area} \times H_{Floc\ filter\ height} \times T_{Theoretical\ floc\ filter\ concentration}}{F_{Total\ clarifier\ influent\ flow\ rate} \times C_{Clay\ clarifier\ influent\ concentration}} \quad \text{Equation 2}$$

## Experiments

An initial experiment was conducted in order to test the rapid growth of a floc filter. Clay stock solution, coagulant, and water were pumped through the tube flocculator and into the clarifier at a total influent flow rate of 1.2 mL/s over the course of 30-45 minutes. An effluent pump was used to prevent the clarifier from overflowing. The clay stock solution had a

concentration of 1300 mg/L, and the coagulant solution had a concentration of 200 mg/L. The same concentrations were used for subsequent experiments. Details regarding flow rates, pump speeds, and concentrations are shown in the table below.

	Clarifier Influent Concentration (mg/L)	Flow Rate (mL/s)	Pump Speed (rpm)
Water		0.928	20.9
Clay Stock	100	0.0923	49.1
Coagulant	30	0.180	91.8

Table 1. Conditions for initial experiment.

Subsequent experiments explored introducing colored particles into the floc filter. The same conditions as in the initial experiment were used to form an uncolored floc filter. Following floc filter formation, a solution of colored clay at a concentration of 536.585 mg/L was added to the system between the flocculator and the clarifier, usually for around 45-60 minutes at a time. Multiple variations on this experiment are detailed below.

<b>Only Rose Clay</b>			
	Clarifier Influent Concentration (mg/L)	Flow Rate (mL/s)	Pump Speed (rpm)
Water		1.09	24.5
Clay Stock	0	0	0
Coagulant	0	0	0
Rose Clay	50	0.112	8.86
<b>Blue Clay + Continued Flocculation</b>			
Water		1.2	27.0
Clay Stock	100	0.0923	49.1
Coagulant	20	0.120	61.2
Blue Clay	300	0.671	53.2
<b>Black Clay + Reduced Flocculation*</b>			
Water		1.01	22.8

Clay Stock	20	0.0185	9.81
Coagulant	4	0.00741	3.78
Black Clay	100	0.16	12.7

\*Coagulant stock solution and black clay solution were 648 mg/L and 750 mg/L for this trial

Table 2. Conditions for experiments with colored primary particles.

An experiment was also performed to investigate coagulant floc formation. Rather than adding clay stock to form flocs, coagulant was added on its own, and the amount added was increased significantly. The concentration of the coagulant stock solution itself was also much higher (600 mg/L instead of 200 mg/L), allowing for even larger doses of coagulant to be added if desired. Primary particles in the form of rose clay solution were then added to the resulting coagulant flocs to test the ability of the flocs to capture particles and perform floc sweeping. Details are shown below.

Coagulant Floc Formation			
	Clarifier Influent Concentration (mg/L)	Flow Rate (mL/s)	Pump Speed (rpm)
Water		1.1	24.8
Clay Stock	0	0	0
Coagulant	50	0.18	51.0
Rose Clay	0	0	0
Coagulant Floc Sweeping			
Water		0.976	22.0
Clay Stock	0	0	0
Coagulant	0	0	0
Rose Clay	100	0.224	17.7

Table 3. Conditions for experiments on coagulant floc formation.

## Results & Analysis

The initial experiment confirmed our ability to form a floc filter within the clarifier. The jet diffuser kept the flocs in suspension, and the plate settlers could be seen aggregating smaller flocs and reintroducing them into the floc filter. There were some issues with wasting from the floc filter into the floc hopper, which could be an area of improvement for future design iterations, but the clarifier was largely successful in maintaining a stable floc filter.



Figure 5. Floc filter formed in clarifier during Initial experiment.

Further experiments with adding colored primary particles after the flocculator also saw success. Over the course of 30-45 minutes, the floc filter could clearly be observed taking on the color of the added primary particles. The blue and rose clay showed the most contrast, while adding black clay formed gray flocs which were difficult to discern from the initial colorless flocs and the gray background of the clarifier. The degree of coloration also varied spatially throughout the floc filter, though subtly, and digital processing was necessary to make the color gradient visible in images. The very bottom of the floc filter usually appeared to be the least colored, though this may be the result of flocs at the bottom of the floc filter not being recirculated due to the geometry of the influent jet. Besides this uncolored region, lower regions in the floc filter tended to be more strongly colored and hence more saturated, with the level of saturation slightly decreasing as height increased.



Figure 6. Enhanced image of coloration in floc filter. The clear spatial variation indicates different levels of saturation throughout.

In addition to these observations on the coloration of the floc filter, the flocs composing the floc filter appeared to shrink over time. The rate at which this occurred seemed related to the coagulant dosage. In one trial, coagulant dosage was decreased mid-experiment due to fear of overdosing after observing large, sticky flocs. After lowering the coagulant dosage, the flocs shrank in size. Furthermore, after flocs shrank to a certain size, they tended to aggregate at the bottom of the floc filter into a sludge. Once this sludge formed, it was extremely difficult to resuspend the flocs as the influent jet tended to carve a narrow channel through it to follow.

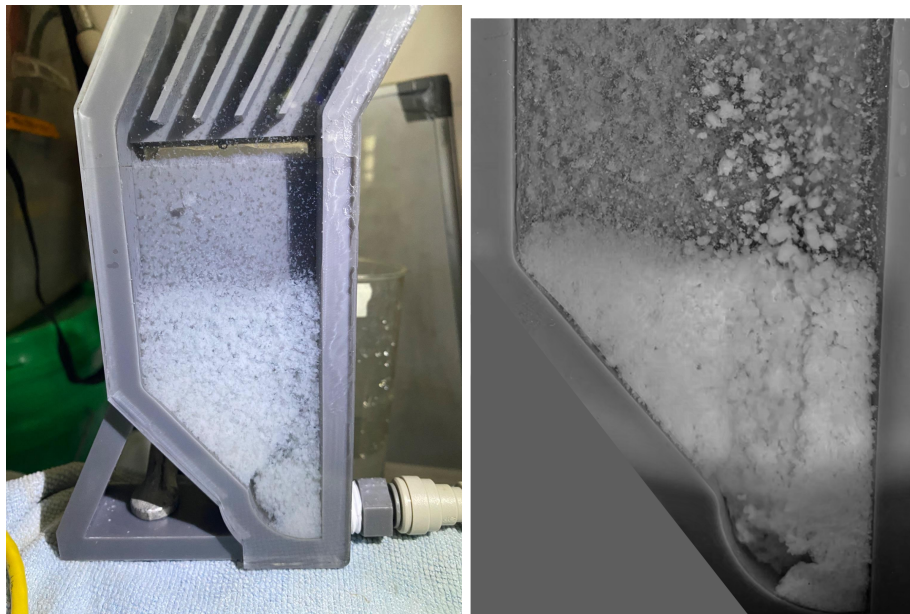


Figure 7. Two instances of the floc filter becoming too tightly packed and failing to remain suspended. The flow forms narrow channels through the dense mass of flocs.

One notable observation regarding this failure to resuspend was that even if the flocs were not allowed to shrink down, if the flocs were intentionally allowed to settle to the bottom of the floc filter by temporarily turning off the influent jet, the flocs would still aggregate into a sludge that could not be resuspended. While allowing the flocs to shrink too much was one way to reach this failure mode, it did not seem to be the only way to reach it.

Populating the floc filter with coagulant flocs seemed to create a similar form of sludge at the bottom of the clarifier. Sending coagulant at a very high concentration through the flocculator by itself was enough to form coagulant flocs, which tended to be irregular in shape and formed long tendrils between neighbors. This naturally aggregated the coagulant flocs into a network within the clarifier. This network stuck to the sides of the diffuser and the walls of the clarifier. Unlike the other floc sludges, the coagulant network did not appear very dense, but it was still very cohesive. When agitated using a piece of tubing inserted into the top of the clarifier, the network remained whole and returned to its original configuration as soon as the tubing was removed.



Figure 8. Coagulant flocs in the clarifier. The coagulant flocs are concentrated at the bottom of the clarifier. Unfortunately, they are difficult to spot on the gray background.

When primary particles were added to the clarifier influent, the coagulant network failed to capture a significant number of particles. In fact, it initially seemed like the clay did not interact with the coagulant flocs at all. After around 30 minutes of running primary particles through the coagulant network and agitating the network, the network began to break apart into individual flocs. Many of these smaller flocs were actually carried into the effluent, possibly due to the lower density of coagulant flocs. The remaining flocs appeared very compact and spherical, and they were the same color as the primary particles used. Over time, they became smaller and settled to the bottom of the clarifier, becoming entirely ineffective as a floc filter.

## Discussion

Sarmiento's previous literature demonstrates a clear indication that clarifier performance decreases over time. Previously, the main explanation for this occurrence was the idea of floc sweeping causing flocs to become more saturated over time, therefore decreasing their removal efficiency as they remained in the clarifier. Our experimentation demonstrated that this mechanism was visible via the color difference in Figure 6 between the resuspended flocs and the flocs that were stuck along the edges of the clarifier. With the addition of blue clay acting as primary particles into the system, the suspended flocs indeed acted like a floc filter and, via internal floc flow, "swept" up enough primary particles to see a coloration difference. The spatial variation indicates that flocs that have been in the floc filter longer have become more saturated.

However, a few other key observations were also made throughout the experiment series. Two experiments where a floc filter was formed, then coagulant addition was temporarily paused, demonstrated flocs becoming more compact. Even after coagulant addition was restarted, Figure 7 demonstrates the aged floc's inability to be resuspended. A few mechanisms could account for this phenomenon, or even act in tandem with each other, including "floc shrinkage" and "coagulant dissolution". Coagulant dissolution is where coagulant previously bonded to clay particles in flocs dissolves into the water around it, driven in particular by the lower coagulant concentration around it, as coagulant addition was paused. Floc shrinkage is the mechanism by which flocs become more compact, potentially due to outside collisions causing particles to come closer together. Coupled with coagulant dissolution, it is possible that flocs become less porous and more compact due to the coagulant providing a mechanism for flocs to be fluffy. With less coagulant, the clay particles within flocs would form bonds with other coagulant particles that haven't been dissolved, but forcing the floc into a more compact structure.

These proposed mechanisms are seen in the Floc Filtration portion of the mechanistic framework seen in Figure 8. The diagram shows that floc shrinkage, coagulant dissolution, and floc sweeping are all continuous mechanisms by which floc aging occurs within the floc filter, which contributes to the overall removal efficiency decreasing. The floc shrinkage and coagulant dissolution mechanisms are located in the same cycle to indicate their potential coupling. The placement of floc sweeping allows it to be the mechanism for Non-Settleable Particles to be uptaken by the floc filter, before there is the possibility of the NSP being caught by the plate settlers.

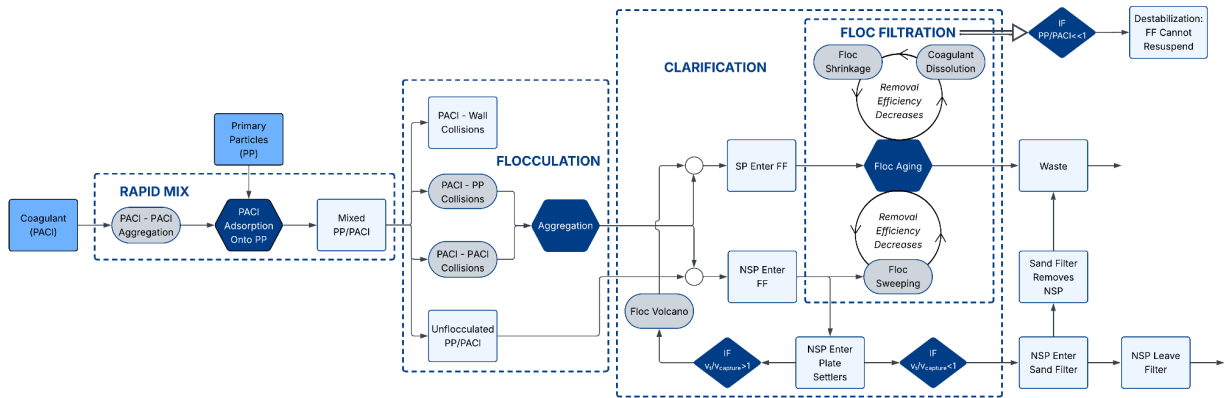


Figure 9. Current mechanistic framework describing rapid mix, flocculation, clarification, and floc filtration processes. Aggregation forms SP (Settleable Particles) and NSP (Non-Settleable Particles).

## Future Work

The team has many ideas for improving the understanding of floc formation, coagulant-clay interactions and mechanisms, floc structure, and floc aging.

Firstly, to gain a better visualization of floc formation mechanisms within the flocculator, an adaptor-like apparatus was designed as seen in Figure 9. The two ends of a tube flocculator can be inserted into either side of the apparatus, allowing the contents of the flocculator to flow through the adaptor. One side of the adaptor will be flat and covered in clear acrylic, allowing a viewer to see directly and clearly into that section of the flocculator. The adaptor also gradually widens, allowing the velocity of the liquid to slow down temporarily for easier visualization throughout the flocculator.

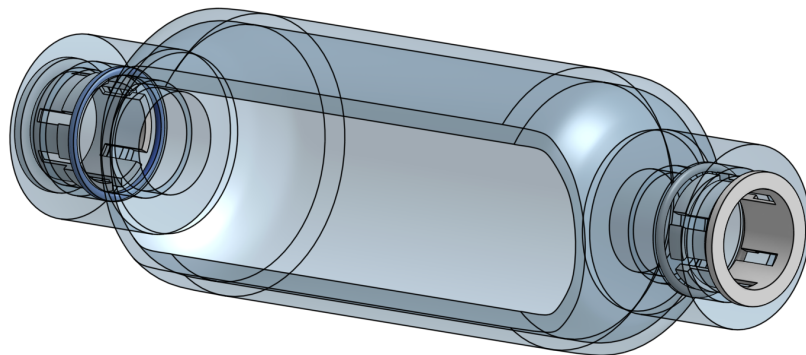


Figure 10. Flocculator window design.

This visualization of flocculation mechanisms will provide insight into how coagulant functions, what a floc looks like throughout formation, and how many different variables (overdosing, underdosing, DOM levels, etc.) could affect how a floc is formed.

A horizontal flow clarifier could also be used to provide insight into floc structure and floc aging. By opposing primary particle flow and floc filter flow horizontally, there could be an equalization of forces where an uptake of primary particles via the floc filter would be able to be observed with much less complicated fluid dynamics compared to the current vertical flow clarifier. This system would allow for a better understanding of floc saturation via empiricism. In this case, a microscope may be able to be used as an additional mechanism of understanding how floc structure changes during floc saturation, due to flocs not moving as much compared to a vertical flow clarifier.

Microscopic analysis could also be used in future experiments to analyze differences in floc structure depending on various conditions. For example, it could provide more insight into the experimental results seen in Figure 7, where the older, non-suspendable flocs have more condensed structures than the new, suspendable flocs. This method could also be applied to experiments where multiple colors of primary particles are used. For example, imaging of flocs saturated by multiple clay colors over time would aid in our understanding of which regions, within a floc, take up primary particles throughout floc saturation. Furthermore, primary particles could be added under different conditions, such as overdosing or no coagulant, and imaged to understand how these conditions affect floc structure.

Finally, the team plans to run systematic experiments with different coagulant doses to gather more empirical evidence and data supporting our understanding of various proposed flocculation and clarification mechanisms.

## Part II: Flocculation Modeling

### Methods

Three models were developed this semester in order to investigate the dynamics of flocculation. The aim of these models is to better understand the rate limiting step(s) of flocculation, account for both diffusion and shear transport processes, and develop a working model for overdosing.

#### Kinetics Model

A kinetics model was developed in Python and describes the collisions between coagulant particles, primary particles and flocs driven by diffusion and shear. It also considers collisions between coagulant particles and the flocculator walls as coagulant particles diffuse through the wall's boundary layer. The populations of these particles are tracked over time. As coagulant particles collide with primary particles and flocs, the fractional surface coverage of the primary particles and flocs changes. This in turn influences the attachment efficiency of subsequent collisions, as attachment efficiency is estimated as being proportional to coagulant surface coverage. Additionally, the average radii of the particle populations changes over time as particles collide, considering fractal growth. The equations and code for this model are provided in [this Google Colab](#).

There are several key assumptions of this model. The model assumes that only like-sized collisions occur between flocs and primary particles, and similarly only like-sized collisions occur between coagulant particles. This is also a critical assumption of the Aguacela Flocculation Model and occurs as a result of the boundary layer induced by shear in the flocculator (Weber-Shirk, n.d.). The model also introduces the idea that bonds can only form if the momentum of the particles colliding is not too large compared to the bond strength ( $E_{bond}$ ). Additionally, as described above, the attachment efficiency between particles is assumed to be proportional to coagulant surface coverage. The model does not currently account for potential phenomena such as local charge reversal that may result in overdosing (see the third flocculation model section below for additional details). Lastly, the model assumes that particle collisions are driven by diffusion and shear in parallel, such that the overall rate constant is the sum of the diffusion and shear rate constants (Swetland et al., 2013). However, this assumption may not be fully accurate and needs to be validated using the second model described below.

### **Advection-Diffusion Model**

In order to investigate how parallel transport mechanisms of diffusion and shear (also known as advection) influences particles collisions, the steady-state spherical advection-diffusion equation can be used to determine how particle concentration varies surrounding a particle of interest (Equation 1). The flux evaluated at the surface of the particle of interest can be used to determine the rate at which collisions occur with that particle.

$$(1) \quad \frac{\delta C}{\delta t} = \nabla \cdot (D \nabla C - \vec{v} C)$$

The equation was numerically solved using the NDSolve function in Wolfram Mathematica. A spherical sink of radius  $R$ , representing the surface of the particle of interest, was placed at the center of the simulation domain. Surrounding it was a spherical source with radius  $R_{bulk}$ , located at a distance where the particle concentration can be reasonably approximated as uniform and equal to the bulk particle concentration. A linear shear velocity profile was simulated in the x-direction as determined by the velocity gradient,  $G$ .

This simulation approach can be setup with any type of spherical particle of interest and bulk particle population. For example, both the particle of interest and the bulk particles could be primary particles. Alternatively, the particle of interest could be a primary particle while the bulk particles are coagulant.

### **Coagulant Overdosing Model**

Flocculation models must account for the experimental observation of overdosing—where adding too much coagulant results in little to no floc formation during flocculation. One theory for this phenomenon is local charge reversal, in which a region on a clay particle with high coagulant coverage may be unable to form a strong bond with a similar

region on another clay particle. This can be explained by the negative surface charge of the clay particle becoming locally positively charged. As a result, collisions may be more likely to result in successful attachment when the collision contact point has one clay surface and one coagulant surface compared to coagulant-coagulant contact. The attachment efficiency ( $\alpha$ ) in the AguaClara Flocculation Model was modified to account for this by introducing two proportionality constants: the fraction of coagulant-coagulant collision that result in successful attachment ( $k_a$ ) and the fraction of coagulant-clay collisions that result in successful attachment ( $k_b$ ).

$$\alpha = f^2(k_a - 2k_b) + 2fk_b \quad (2)$$

$$f = \min(k' \frac{C_{coag}}{C_{influent}}, 1) \quad (3)$$

## Results & Analysis

The kinetics model was simulated with an initial coagulant concentration of 20 mg/L and primary particle concentration of 100 mg/L. The coagulant began aggregating for one second prior to aggregating with primary particles, in order to simulate the time between coagulant injection and mixing with the surrounding fluid. The maximum number of primary particles per floc was set to be  $2^{11}$ , or 2,048, particles based on the estimated maximum size of a floc before gravity breaks it apart (Weber-Shirk, n.d.). This resulted in the following trends over time (Figure 11).

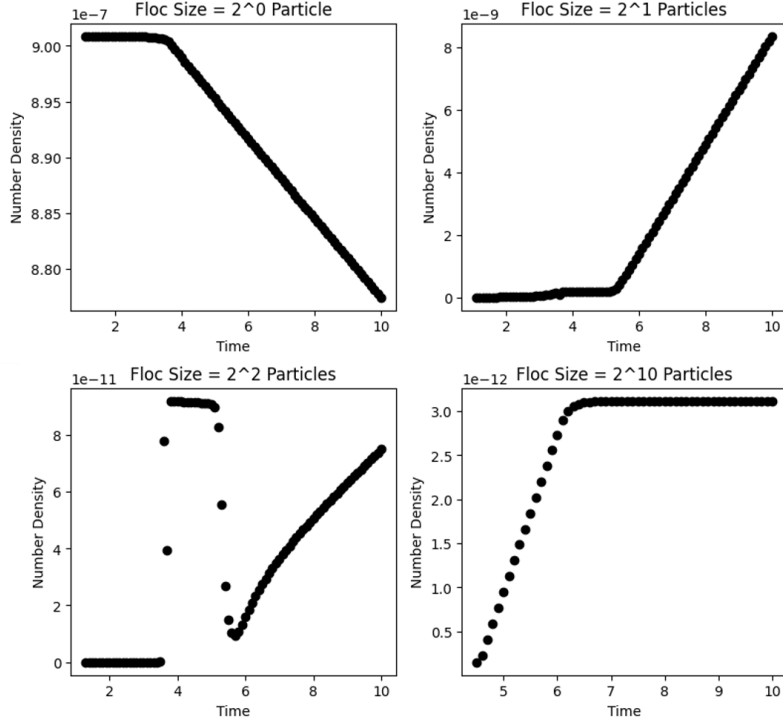


Figure 11. Number density ( $1/\text{micrometer}^3$ ) over time of select primary particle and floc sizes.

The advection-diffusion model was simulated for collisions between primary particles at a bulk concentration of 10 mg/L. A velocity gradient,  $G$ , of 10 Hz was used, and 10 times the mean free path between primary particles was chosen as the  $R_{bulk}$  value of 1.04 millimeters. This resulted in an expected time of collision of 0.000044 seconds. This is the expected time for any primary particle to collide with a given primary particle of interest.

The overdosing model was manually fit to data from Pennock et al., 2018, with a  $k_a$  value of 0.1 and  $k_b$  value of 1. In order to match the experimental conditions used in Pennock et al., 2018, this model was simulated with an influent turbidity of 300 mg/L, mean velocity gradient ( $G$ ) of 147 Hz, and flocculator hydraulic residence time of 413 seconds. This resulted in the following fit (Figure 12).

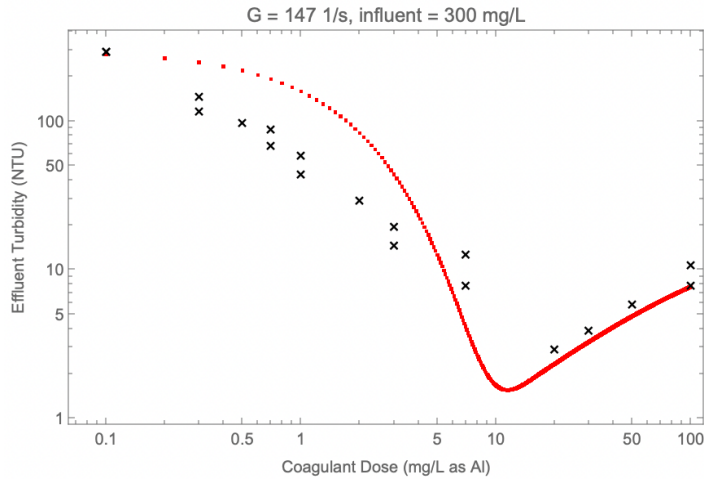


Figure 12. Manual fit of the overdosing model. Data adapted from Pennock et al., 2018.

## Discussion & Future Work

The results from the kinetics model suggest that the initial steps of aggregation between the smallest primary particles may be the rate limiting step to flocculation. The population of the larger flocs tends to quickly approach steady-state at very small values, while the first few populations of particles (containing 1-4 primary particles) follow a more transient response and appear to continue growing in population over a larger time period. This indicates that these smaller particles collide to form larger particles at a slower rate than the larger particles colliding with each other. This supports the fundamental assumption of the AguaClara Flocculation Model.

However, the simulation was only conducted for one set of influent and coagulant concentrations and should be conducted across a range of concentrations in order to determine whether the rate limiting step varies. Additionally, based on Swetland et al., 2013, faster rapid mix results in smaller coagulant aggregates which can increase coagulant surface coverage and thereby improve attachment efficiency. This model may therefore enable predictions regarding how fast the initial rapid mix of coagulant should occur in order to optimize coagulant usage. In order to further improve this model, the overdosing term from the third model could be incorporated when calculating attachment efficiency. The advection-diffusion model should also be simulated at various concentration values and particle sizes. The results can then inform the rate constant values from the kinetics model and determine whether the predicted collision times in the kinetics model are reasonable.

The overdosing model currently does not provide an accurate fit with experimental data when using theoretically appropriate values for the constant  $k'$ . This suggests the model is missing a critical component that needs to be determined. In collaboration with the ACDC subteam, future experimentation will be conducted in order to strategically investigate overdosing failure. Quantitative data of flocculation performance will be collected and coupled to model predictions.

# Part III: Clarification Modeling

## Methods

As described in the Literature Review section and Appendix Section I, the working model of floc sweeping and floc saturation contained a discrepancy between the theoretical and experimentally-fitted values of the constant  $k_c$ . This suggested the model was missing a critical component. This semester, the team corrected for the calculation of  $k_c$  and modified the calculation of clarification attachment efficiency. See Appendix Section I for an overview of the model, which couples the AguaClara Flocculation Model with a model for floc sweeping and floc saturation.

$C_{flocFilter}$  is a value included in  $k_c$  that describes the concentration of flocs within the floc filter.  $C_{flocFilter}$  is assumed to be a constant, as supported by fluidized bed theory. This constant was previously estimated as approximately 3000 mg/L based on the work of Hurst et al., 2014, resulting in a  $k_c$  value on the order of 0.001. However, experimental fitting of operator data from an AguaClara treatment plant in Nicaragua suggested a value for  $k_c$  on the order of 1000.

This discrepancy is the result of an error between distinguishing the concentration of clay from the concentration of flocs in the floc filter; 3000 mg/L is the concentration of clay in the floc filter, not the concentration of flocs. This is an important distinction, as a majority of a floc's volume is composed of water rather than clay due to its fractal structure.

Additionally, the clarification model used the same attachment efficiency as the flocculation model described above while assuming that each primary particle only collides once with a given floc. However, this description misses key aspects of the floc sweeping process in the floc filter. Specifically, water and primary particles flow through channels internal to flocs as they flow upwards through the floc filter. Given the significantly larger size of flocs compared to primary particles, this process is expected to result in several collisions between a given primary particle and a given floc. As a result, the equation for the attachment efficiency between primary particles and flocs in the floc filter was modified to include a value,  $n$ , describing the average number of collisions as a primary particle interacts with a given floc.

Lastly, a theoretical value for the flocculation constant,  $k_{pf}$ , was incorporated based on the predicted fractional coverage of primary particles with coagulant, given a primary particle diameter on the order of 1 micrometer and a coagulant particle diameter on the order of 100 nm (Equation 7). This coagulant particle size was determined in Swetland et al., 2013. These modifications resulted in the following equations:

(4)

$$C_{clarified} = C_{flocculated} e^{-k_c \alpha_c h_{floc filter}} \text{ where } k_c = \frac{\pi r_{floc}^2 C_{floc filter}}{m_{floc}}$$

(5)

$$\alpha_c = 1 - (1 - k' \frac{C_{coagulant}}{C_{influent}} (1 - P_{floc\ saturated})^{\frac{2}{3}})^n \quad (6)$$

$$C_{flocculated} = (\frac{C_{coagulant}}{k_{pf} C_{influent}} + C_{influent})^{-2/3}^{-3/2} \text{ where } k_{pf} = \frac{3}{2\pi k' G\theta} (\rho \frac{\pi}{6})^{2/3} \quad (7)$$

$$k' = \frac{\rho_{clay}}{4\rho_{coagulant} (\frac{(r_{clay} + r_{coagulant})^2}{r_{coagulant}})}$$

## Results & Analysis

By accounting for the difference between the concentration of clay and the concentration of flocs, the recalculated value of  $k_c$  is on the order of 1000. Additionally, the theoretical value of  $k'$  is 0.00063, such that the theoretical value of  $k_{pf}$  is 0.011. Using these values results in a model curve that closely matches experimental data (Figure 13). In order to achieve this, the unknown constants  $q$ ,  $n$ , and  $k$  were adjusted to manually fit the model to the experimental data, resulting in a  $q$  value of 0.55,  $n$  value of 200, and  $k$  value of 0.41.

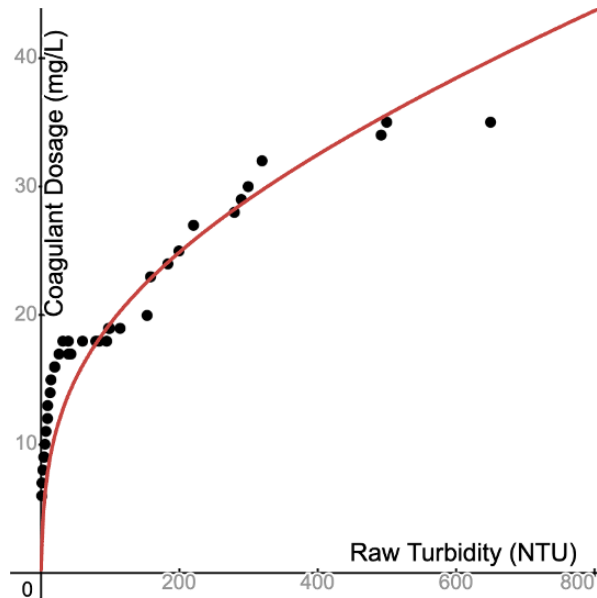


Figure 13. Clarification model fit to operator data from an Aguac Clara plant in Nicaragua.

## Discussion

The match between the model curve and experimental data described above suggests the model may be a reasonable representation of the coupled dynamics of flocculation and clarification. However, there remains a critical aspect of the given experimental dataset that the model does not account for: the apparent difference in curvature between the low influent turbidity and high influent turbidity regimes. Specifically, there appears to be an inflection point

at an influent turbidity of approximately 60 NTU. It is difficult to fully explore why this phenomena is occurring, as this dataset does not indicate potential confounding variables including the presence of dissolved organic matter (DOM) in the water, during which data points operators are wasting from the floc filter, which data points are from the dry versus rainy season, and what the resulting clarified turbidity is for each data point. All of these variables will play a significant role in model predictions and may be able to explain this phenomena. However, more data collected in a controlled environment is necessary to fully validate this model and understand the origin of this phenomena. Nevertheless, the ability for this model to generally follow trends from a real-world Aguacalera treatment plant is highly promising.

## Future Work

Observations from the floc saturation experiments described above will be used to inform future modifications to this clarification model. Specifically, the model will be adjusted to account for a spatial gradient in floc saturation within the floc filter, if experimental results indicate this occurs. Additionally, data on coagulant dose, influent turbidity and clarified turbidity will be collected using the mini-clarifier apparatus and will be compared with model predictions. The phenomena described in the discussion section above will be further investigated using the new data that will be collected.

## Appendix

### Section I: Current Clarification Model

Currently, it is defined that

(A1)

$$C_{clarified} = C_{flocculated} e^{-k_c \frac{C_{coagulant}}{C_{influent}} (1 - P_{floc\ saturated})^{2/3} h_{floc\ filter}} \text{ where } k_c = k' \beta \frac{\pi r_f^2 C_{floc\ filter}}{m_{floc}}$$

(A2)

$$C_{flocculated} = \left( \frac{C_{coagulant}}{k_{pf} C_{influent}} + C_{influent} \right)^{-2/3}^{-3/2} \text{ where } k_{pf} = \frac{3}{2\pi k k' G \theta} (\rho \frac{\pi}{6})^{2/3}$$

(A3)

$$P_{floc\ saturated} = \frac{C_{flocculated} - C_{clarified}}{q(C_{influent} - C_{clarified})}$$

(A4)

$$C_{coagulant} = C_{coagulant\ added} - \lambda C_{DOM}$$

where  $\lambda$ ,  $k$ ,  $k'$ , and  $\beta$  are proportionality constants,  $G$  is the mean velocity gradient in the flocculator,  $\rho$  is the density of clay primary particles,  $\theta$  is the flocculation residence time, and  $q$  is the maximum total mass of primary particles collected per floc in the floc filter.

The value of the constant,  $k_c$ , (see Equation A1) suggests there is a critical component missing from this clarification model. When fitting the model to Aguacalera plant data from La

Concordia Nicaragua, the fitted and theoretical values of  $k_c$  are orders of magnitude off—with 0.0016 as the theoretical value and 1000 as the fitted value.

## Section II: Mass Balance Calculations for Experimentation

Total clarifier influent flow rate (mL/s)	1.2
Effluent flow rate (mL/s)	1.2
Clay/coagulant/red clay clarifier influent flow rate (mL/s)	x
Clay/coagulant/red clay flocculator influent concentration (M)	i
Clay/coagulant/red clay clarifier influent concentration (M)	c
Clay/coagulant/red clay stock concentration (M)	s
Clay/coagulant/red clay pump volume per revolution (mL/rev)	n
Clay/coagulant/red clay pump speed (rev/s)	v
Total flocculator influent flow rate (mL/s)	f
Water flow rate (mL/s)	w
Waste flow rate (mL/s)	a
Effluent with wasting flow rate (mL/s)	e

The equations below found the flow rates and pump speeds during the experiment.

$$\begin{aligned}
 & (A5-A9) \\
 x &= \frac{1.2 c}{s} \\
 v &= \frac{60 x}{n} \\
 f &= 1.2 - w \\
 i &= \frac{s x}{f} \\
 e &= 1.2 - a
 \end{aligned}$$

### Section III: Apparatus Specifications

PUMPS			
Name	ID	Tubing Size	Volume per Rev (mL/rev)
Clay	2	2mm	0.112866
Water	3	17 (6.4mm ID) (# MasterFlex 06508-17)	2.66327
Rose Clay	9	1.65mm	0.0259664
Coagulant	1	2mm	0.117623
Waste	5	16 (1/8" ID) (# MasterFlex 06508-16)	0.849814
Effluent	8	17 (6.4mm ID) (# MasterFlex 06508-17)	2.785

TURBIDIMETERS	
Name	ID
Influent	7
Clarified	6

Figure A1. Pump and turbidimeter specifications. The volumes per revolution were determined manually.

## Manual

### Experiment SOP

#### Creating stock solutions

Stock solutions were created and stored in 1 L bottles. Magnetic stir bars were placed in the white and colored clay stock solutions because the clay settles to the bottom over time.

#### Pumps and Machines

Insert the tubes connected to pumps into the corresponding bottles of stock solution. Turn on the water pipe by turning the water lever in Hollister B60 until it is perpendicular. Then, turn on the lab computer, turbidimeters, and all pumps. Using the “Just water with Effluent” state (see next section), run water through the system for ten minutes to flush out residual chemicals.

#### ProCoDA

Open ProCoDA and use the method file “ProCoDA 0” in the folder in Floc Modeling SP25. There are five states:

1. “Run without wasting” runs coagulant, white clay, water, rose clay, and effluent pumps.

2. “Just water no Effluent” runs water and waste pumps.
3. “Just water with Effluent” runs water, effluent, and waste pumps.
4. “Run with wasting” runs coagulant, white clay, water, rose clay, waste, and effluent pumps.
5. “Floc filter growth” runs coagulant, clay, water, and effluent pumps. This state can be used to grow the initial floc filter because it runs at a higher pump speed to rapidly increase influent concentrations.

### **Cleanup**

When experiments have concluded, turn off pumps, turbidimeters, and the lab computer. Empty the clarifier, and seal stock solution bottles. Coagulant stock solution with low concentration will lose effectiveness over time. Thus, replace the coagulant stock solution often.

### **Troubleshooting**

If there are air bubbles entering the clarifier, poke a needle into the tube or insert a smaller tube to release air. Furthermore, raising the lower end of the tube leverages pressure differences to purge air bubbles. If pumps or turbidimeters are not connecting to the computer, turn them off and restart ProCoDA; ensure that the ID's and settings on ProCoDA are correct. If turbidimeter readings are inaccurate, check and clean the turbidimeter for residual particles and/or recalibrate the device.

### **Mini-Clarifier Fabrication**

The main body of the mini-clarifier was resin-printed in three separate parts at Cornell’s Rapid Prototyping Lab: the diffuser, the plate settlers, and the floc hopper. These parts were assembled and glued together using epoxy. The acrylic plates used for the front of the clarifier and the back of the floc hopper were laser cut and also attached using epoxy. The influent jet nozzle was not epoxied into place; rather, it was threaded into the main body using teflon tape to allow for future modifications. In order to attach tubing to different points on the mini-clarifier including the influent nozzle, overflow tube, effluent tube, and waste tube, threaded adapters were used to self-tap these holes. Some holes required additional drilling in order to accommodate the adapter.

## **References**

Argaman, Y., & Kaufman, W. J. (1970). Turbulence and flocculation. *Journal of the Sanitary Engineering Division*, 96(2), 223–241. <https://doi.org/10.1061/jsedai.0001073>

Bridgeman, J., Jefferson, B., & Parsons, S. A. (2009). Computational Fluid Dynamics Modelling of Flocculation in Water Treatment: A review. *Engineering Applications of*

*Computational Fluid Mechanics*, 3(2), 220–241.  
<https://doi.org/10.1080/19942060.2009.11015267>

Casson, L. W. and Lawler, D. F. (1990) Flocculation in Turbulent Flow: Measurement and Modeling of Particle Size Distributions. *J. American Water Works Association*, 82, 54-68.

Chen, L. C., Lee, D. J., Chou, S. S. (2006). Charge Reversal Effect on Blanket in Full-Scale Floc Blanket Clarifier. *Journal of Environmental Engineering*, 132(11).  
[https://doi.org/10.1061/\(ASCE\)0733-9372\(2006\)132:11\(1523\)](https://doi.org/10.1061/(ASCE)0733-9372(2006)132:11(1523))

Du, Y., Pennock, W. H., Weber-Shirk, M. L., & Lion, L. W. (2019). Observations and a geometric explanation of effects of humic acid on flocculation. *Environmental Engineering Science*, 36(5), 614–622. <https://doi.org/10.1089/ees.2018.0405>

Gernaey, K., Vanrolleghem, P. A., & Lessard, P. (2001). Modeling of a reactive primary clarifier. *Water Science & Technology*, 43(7), 73–81. <https://doi.org/10.2166/wst.2001.0393>

Haarhoff, J., & Joubert, H. (1997). Determination of aggregation and breakup constants during flocculation. *Water Science & Technology*, 36(4).  
[https://doi.org/10.1016/s0273-1223\(97\)00416-2](https://doi.org/10.1016/s0273-1223(97)00416-2)

Head, R., Hart, J., & Graham, N. (1997). Simulating the effect of blanket characteristics on the floc blanket clarification process. *Water Science & Technology*, 36(4).  
[https://doi.org/10.1016/s0273-1223\(97\)00422-8](https://doi.org/10.1016/s0273-1223(97)00422-8)

Liu, J., Crapper, M., & McConnachie, G. (2004). An accurate approach to the design of channel hydraulic flocculators. *Water Research*, 38(4), 875–886.  
<https://doi.org/10.1016/j.watres.2003.10.014>

Pennock, W. H., Weber-Shirk, M. L., & Lion, L. W. (2018). A hydrodynamic and surface coverage model capable of predicting settled effluent turbidity subsequent to hydraulic flocculation. *Environmental Engineering Science*, 35(12), 1273–1285.  
<https://doi.org/10.1089/ees.2017.0332>

Runkana, V., Somasundaran, P., & Kapur, P. C. (2004). Mathematical modeling of polymer-induced flocculation by charge neutralization. *Journal of Colloid and Interface Science*, 270(2), 347-358. <https://doi.org/10.1016/j.jcis.2003.08.076>

Sarmiento, K. (2021). Particle Removal in Floc Blanket Clarifiers Via Internal Flow Through Porous Fractal Aggregates. *Cornell University*.

Shammas, N.K. (2005). Coagulation and Flocculation. In: Wang, L.K., Hung, YT., Shammas, N.K. (eds) Physicochemical Treatment Processes. *Handbook of Environmental Engineering*, 3(103-139). Humana Press. <https://doi.org/10.1385/1-59259-820-x:103>

- Smoluchowski, M. (1917) Mathematical Theory of the Kinetics of the Coagulation of Colloidal Solutions. *Zeitschrift für Physikalische Chemie*, 19, 129-135.
- Swetland, K. A., Weber-Shirk, M. L., Lion, L. W. (2013). Influence of Polymeric Aluminum Oxyhydroxide Precipitate-Aggregation on Flocculation Performance. *Environmental Engineering Science*, 30(9). <https://doi.org/10.1089/ees.2012.0199>
- Swetland, K. A., Weber-Shirk, M. L., Lion, L. W. (2014). Flocculation-Sedimentation Performance Model for Laminar-Flow Hydraulic Flocculation with Polyaluminum Chloride and Aluminum Sulfate Coagulants. *Journal of Environmental Engineering*, 140(3). [https://doi.org/10.1061/\(ASCE\)EE.1943-7870.0000814](https://doi.org/10.1061/(ASCE)EE.1943-7870.0000814)
- Takács, I., Patry, G., & Nolasco, D. (1991). A dynamic model of the clarification-thickening process. *Water Research*, 25(10), 1263–1271. [https://doi.org/10.1016/0043-1354\(91\)90066-y](https://doi.org/10.1016/0043-1354(91)90066-y)
- Tse, I. C., Swetland, K., Weber-Shirk, M. L., & Lion, L. W. (2011). Fluid shear influences on the performance of hydraulic flocculation systems. *Water Research*, 45(17), 5412–5418. <https://doi.org/10.1016/j.watres.2011.07.040>
- Vitasovic, Z. Z. (1986). An Integrated Control Strategy for the Activated Sludge Process. Rice University.
- Weber-Shirk, M. (n.d.). *The Physics Of Water Treatment Design*. <https://aguaclara.github.io/Textbook/index.html>